Ramirez Hoyos, P.; Manzanares, JA.; Cervera Montesinos, J.; Gómez Lozano, V.; Ali, M.; Pause, I.; Ensinger, W.... (2018). Nanopore charge inversion and current-voltage curves in mixtures of asymmetric electrolytes. Journal of Membrane Science. 563:633-642. doi:10.1016/j.memsci.2018.06.032

Nanopore charge inversion and current-voltage curves in mixtures of asymmetric electrolytes

Patricio Ramirez,[1,*] José A. Manzanares,[2] Javier Cervera,[2] Vicente Gomez,[1] Mubarak Ali,[3,4] Isabelle Pause,[4] Wolfgang Ensinger,[4] and Salvador Mafe[2]

[1]*Departament de Física Aplicada, Universitat Politécnica de València, E-46022 València (Spain)*

[2]*Departament de Física de la Terra i Termodinàmica, Universitat de València, E-46100 Burjassot (Spain)*

[3]*Materials Research Department, GSI Helmholtzzentrum für Schwerionenforschung, D-64287 Darmstadt (Germany)*

[4]*Department of Material- and Geo-Sciences, Technische Universität Darmstadt, D-64287 Darmstadt (Germany)*

ABSTRACT

We consider the screening of the negative charges (carboxylic acid groups) fixed on the surface of a conical-shaped track-etched nanopore by divalent magnesium (Mg^{2+}) and trivalent lanthanum (La^{3+}). The experimental current (I)–voltage (V) curves and current rectification ratios allow discussing fundamental questions about the overcompensation of spatially-fixed charges by multivalent ions over nanoscale volumes. The effects of *charge inversion* or *reversal* on nanopore transport are discussed in mixtures of asymmetric electrolytes ($LaCl_3$ and $MgCl_2$ with KCl). In particular, pore charge inversion is demonstrated for La^{3+} as well as for mixtures of this trivalent ion at low concentrations with monovalent potassium (K^+) and divalent Mg^{2+} ions at biologically relevant concentrations. It is found that small concentrations of multivalent ions can modulate the nanopore rectification and the transport of other majority ions in the solution. We study also the kinetics of the nanopore electrical recovery when the electrolyte solutions bathing the single-pore membrane are changed and show the hysteretic effects observed in the I–V curves. Finally, we describe the hysteresis observed in the I–V curves of $CaCl_2$, $MgCl_2$, and $BaCl_2$ and mixtures. We also give a qualitative description of the effects of charge reversal on the pore rectification using the Nernst-Planck flux equations for multivalent ion mixtures.

Keywords: Charged nanopore; Current-voltage curve; Asymmetric electrolytes, Charge inversion; Current rectification

1. Introduction

The interaction between the negatively charged head groups of the phospholipid molecules forming the cell membrane and the multivalent cations in solution is central to gene delivery, viral packing, and drug action processes. The screening of the charged groups by these ions can produce an electrical overcompensation usually referred to as *charge inversion* or *charge reversal* [1]. Remarkably, the aqueous ion channels inserted between these phospholipid molecules have also fixed charge groups that can interact with divalent and trivalent ions [2]. For wide biological channels such as pore forming toxins and porins, electrical interactions and charge inversion effects are significant [3-5] and depend also on the pH because of the pore fixed charges [6-8]. Partial ion blocking and charge reversal have also been reported in artificial nanopores where small amounts of multivalent ions can modify the electric current transported by other monovalent ions in solution because of their interaction with the groups fixed to the pore surface [9-13].

Charge inversion constitutes a subject of current interest for both fundamental and applied research [1,14,15]. Theoretically, this effect can be studied by means of computer simulations and physical models based on strongly correlated liquids of multivalent ions in the vicinity of a charged surface [1,16-19]. Experimentally, charge reversal can be detected by electrophoresis when a charged colloid in solutions of multivalent ions shows a reversed mobility; see Semenov et al. [20] and Quesada-Perez *et al.* [21] for a review. Alternatively, X-ray reflectivity [22] and atomic force microscope [23] techniques can allow direct measurements of the charge inversion by multivalent counter ions at a charged wall. Artificial nanopores can also be employed to explore charge reversal in confined geometries that resemble those found in biological pores [9-12,24,25].

We consider here the electrical interaction of divalent and trivalent cations with the negatively charged groups at the surface of a conical-shaped track-etched nanopore. This

problem illustrates basic questions about charge inversion and may also suggest new nanopore applications in biosensors and lab-on-a-chip devices because small concentrations of multivalent ions allow tuning the transport of other majority ions present in solution. Indeed, previous work by Siwy et al. [9-11] has shown that because of the high surface-to-volume ratio of nanopores, the pore charges interact strongly with the mobile multivalent ions forming effective ion pairs. In particular, current fluctuations, negative resistance, and precipitation-induced effects have been reported in calcium solutions immersed in narrow pores [9,11]. Under certain conditions, charge inversion can reverse the electrical rectification properties of the nanopore [10]. The sign reversal of the surface charge of rectangular silica nanochannels has previously been studied in mixtures of monovalent and multivalent ions by measuring streaming currents under pressure-driven transport [26]. At high monovalent ion concentrations, the electrical screening can suppress charge inversion and restore the original sign of the surface charge [26]. Reversal (open) potential and conductance measurements have also been reported for divalent (magnesium) ions in nanochannels [25]. Charge inversion was observed together with an anomalous increase of the channel conductivity [25]. The interaction of the negative fixed charges at the pore surface with divalent anions rather than cations has recently been studied [24]. In this case, however, the divalent ions are excluded from the pore and no charge inversion is observed.

We focus here on the conical nanopore charge inversion shown by the current (I)–voltage (V) curves (see Fig. 1) in mixtures of asymmetric electrolytes, including $LaCl_3$ and $MgCl_2$, and KCl. The negative charge of the nanopore results from the dissociation of the carboxylic acid groups fixed to the pore surface. Lanthanum (La^{3+}) is a trivalent ion that can act as a specific blocker of biological ion channels, modulating their electrical characteristics [6]. Magnesium (Mg^{2+}) and potassium (K^+) cations are usually found in biological cells and the carboxylic acid groups are typical chemical moieties of protein ion channels [2]. Mixtures

of asymmetric electrolytes including monovalent and divalent ions are also typical of transport processes through negatively-charged mono and multilayer cation exchange membranes (see [27] and references therein). We study the changes observed in the pore fixed charges, including the electrical screening and overcompensation of these charges, as well as the effects caused by salt addition. We show also the hysteretic effects observed in the *I–V* curves of different multivalent ions and mixtures. A qualitative description of the effects of the charge reversal on the pore rectification is given on the basis of an ad hoc charge distribution (*Appendix A*) and the Nernst-Planck equations (*Appendix B*).

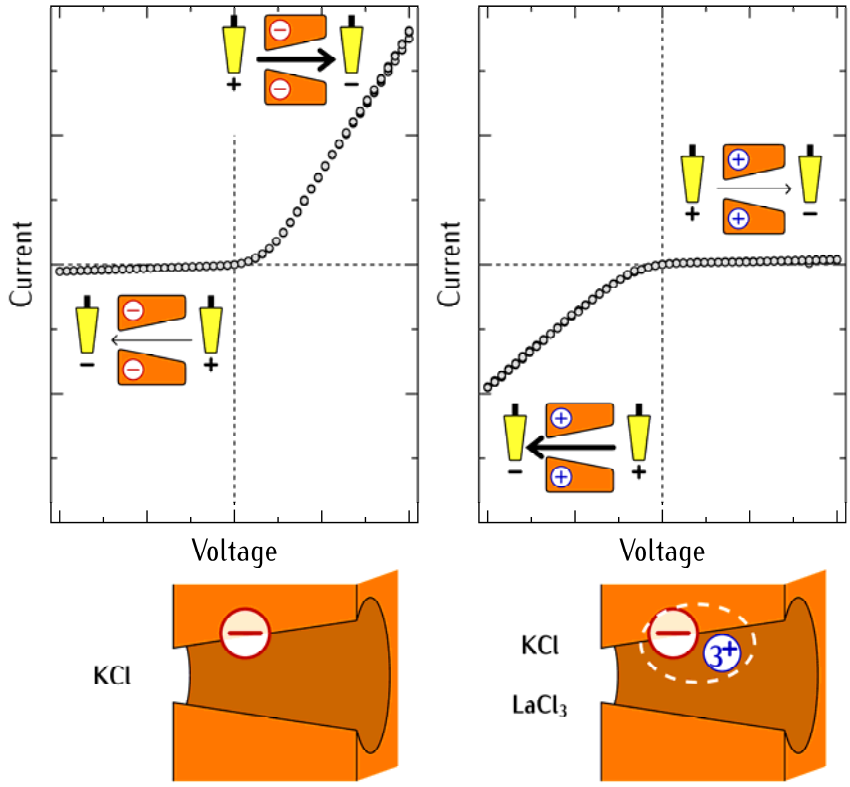

Fig. 1 Scheme of the charge reversal effect observed in the *I–V* curves of the nanopore due to the presence of La^{3+} in the external solutions.

2. Experimental

2.1 Single-pore membranes

Membrane samples that contain the single nanopores are obtained from stacks of 12.5-μm thick polyimide (PI) foils (Kapton50 HN, DuPont). The foils are irradiated at the linear accelerator *UNILAC* (GSI, Darmstadt) with swift heavy ions (Au) of energy 11.4 MeV per nucleon. A metal mask with a 200 micrometer-diameter centered aperture is placed in front of each stack to achieve single-ion irradiation. After a single ion passes through the foil stack and is registered by a particle detector placed behind the samples, the ion beam is blocked immediately. The membrane tracks are converted into approximately conical pores by asymmetric track-etching techniques [28-30]. The SEM images of the nanopore fracture, gold replicas of the conical pores, and nanopore conductances show typical pore radii that are in the range 300–800 nm for the cone base and 10–40 nm for the cone tip [31]. The track-etching process gives carboxylate residues on the pore surface that can be in ionized form at physiological pH in aqueous solutions [28,32].

2.2 Current–voltage (I–V) measurements

The potentiostat/galvanostat BioLogic SP-200 is used for the input (triangular wave) potential and for measuring the current. The single-pore membranes are bathed by $LaCl_3$, $MgCl_2$, and KCl aqueous electrolyte solutions under controlled pH conditions. A couple of Ag|AgCl electrodes in the two bathing solutions allow introducing the input potentials and obtain the output currents. The *I–V* curves of the negatively charged pore show low resistances at positive potentials (currents entering the cone tip) and high resistances at negative potentials (currents entering the cone base) [31–33]. Fig. 1 shows a scheme of the effect of charge reversal on these curves.

3. Results and Discussion

The experimental data reported were obtained with two PI samples containing a single asymmetric pore. Sample 1 was used in the experiments of Fig. 2–6 and Figs. 7a and 7b. Sample 2 was used in Figs. 7c–h and 8. We selected these two samples because they showed almost identical *I*–*V* curves in 100 mM KCl, suggesting similar geometric properties. Hysteresis effects can be important under some experimental conditions [34,35]. The experiments were performed using 14 mHz full triangle waves. In Figs. 2–5 and Figs. 7 and 8, the measurements of each *I*–*V* curve took four periods (*ca.* 300 s = 5 min). Therefore, each current was measured during four ascending and four descending linear ramps, eight times in total.

The pore geometry and fixed charge concentration can be inferred from the comparison of the experimental *I*–*V* curves with a theoretical model previously developed by us [32,33]. We obtained 700 nm (pore base diameter), 35 nm (pore tip diameter) and –0.9 e/nm^2 for the surface fixed charge concentration, where e is the elementary charge. The salt concentration influences the rectification properties (see, e.g., the case of PET nanopores in KCl and $MgCl_2$ solutions [36]). At low concentrations of the external solutions, the nanopore conductance is modulated by the effective concentration of fixed charges on the pore surface [32]. Indeed, because of the co-ion exclusion from the pore, the mobile counter-ion compensating for these fixed charges acts as the majority mobile carrier. The co-ion is the ion having the same sign of the pore fixed charges while the counter-ion is the ion of opposite sign. In the case of the as-prepared pore, the negative pore surface is due to the presence of dissociated carboxylic acid groups. Thus, the monovalent cation (K^+) is the counter-ion while the anion (Cl^-) is the co-ion. However, the effective negative charge of the pore can be partially decreased by the divalent cation (Mg^{2+}) screening. The trivalent cation (La^{3+}) may be expected to go a step further and reverse the sign of the effective pore charge from negative to

positive at sufficiently high concentrations. In this case, the monovalent anion (Cl^-) acts as the counter-ion.

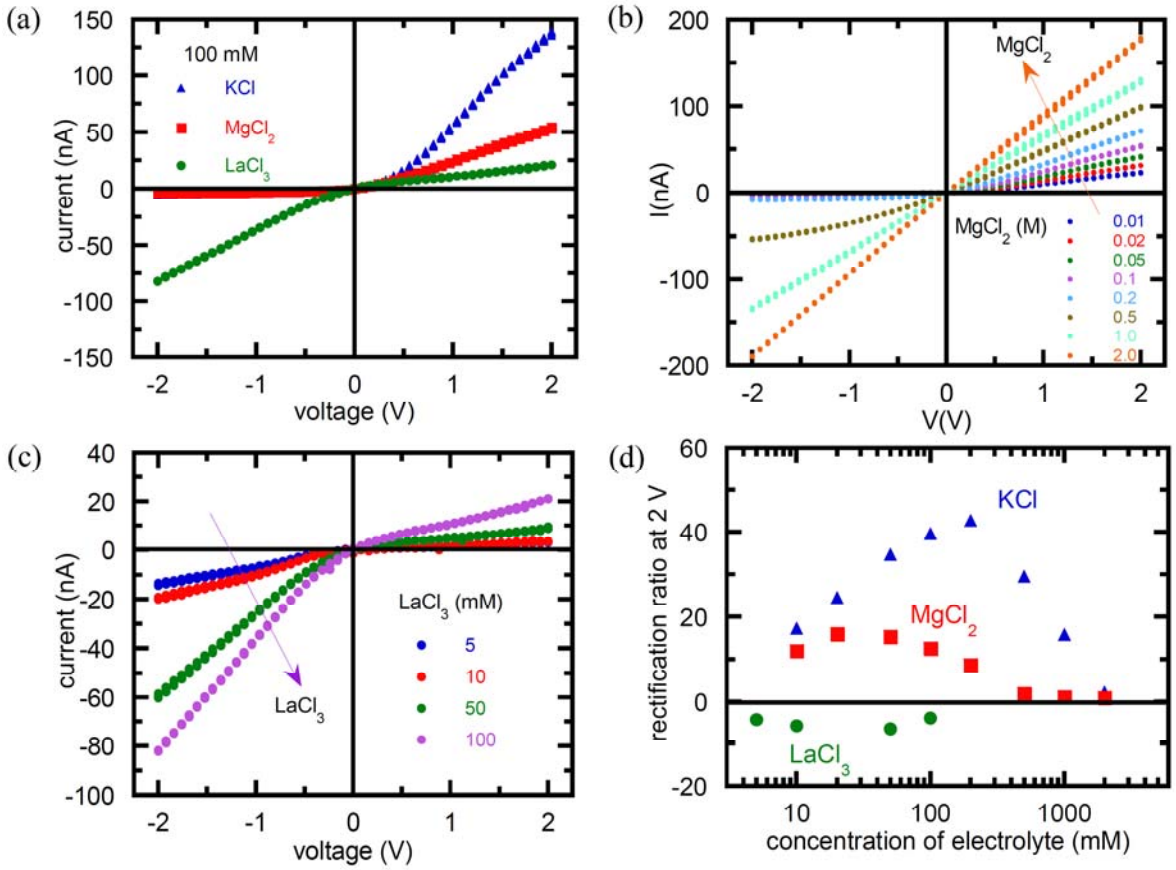

Fig. 2 (a) The *I*–*V* curves of KCl, $MgCl_2$, and $LaCl_3$. The reversal observed in the electrical rectification of the $LaCl_3$ curve suggests an inversion in the pore surface charge from negative to positive. (b) The *I*–*V* curves over a wide range of $MgCl_2$ concentrations demonstrate that this charge overcompensation does not occur. The arrow indicates the direction of increasing $MgCl_2$ concentration. (c) Charge reversal is observed for $LaCl_3$ concentrations higher than 5 mM. The arrow indicates the direction of increasing $LaCl_3$ concentration (d). The electrical rectification ratios $r = \left| I(+2\ \mathrm{V}) / I(-2\ \mathrm{V}) \right| > 1$ for KCl and $MgCl_2$ and $r = I(-2\ \mathrm{V}) / I(+2\ \mathrm{V}) < -1$ for $LaCl_3$ as a function of the electrolyte concentration. The position of the maxima shifts with the cation charge number because of the different number of charges contributing to the pore conductance in each case.

Fig. 2a shows the *I–V* curves of the three electrolytes used which follow the ionic conductance order KCl > $MgCl_2$> $LaCl_3$ for the high conductive branch of the curve. On the contrary, the low conductance branch follows the order $LaCl_3$ > $MgCl_2$ = KCl. Note the inverse rectification observed for the case of $LaCl_3$ with respect to that of $MgCl_2$. This fact suggests a reversal in the pore surface charge from negative to positive for the La^{3+} cation [6,7]. To check the possibility of charge inversion also with the divalent Mg^{2+} cation, Fig. 2b shows the *I–V* curves for $MgCl_2$ at concentrations as high as 2 M where the screening of the pore fixed charges due to the mobile ions in solution suppress the electrical rectification (no charge reversal). On the contrary, the *I–V* curves of Fig. 2c suggest that this reversal can occur for the case of La^{3+} even at lower concentrations (5 mM). Fig. 2d shows the electrical rectification ratios, defined as $r = \left| I(+2\ \mathrm{V}) / I(-2\ \mathrm{V}) \right| > 1$ for KCl and $MgCl_2$ and $r = I(-2\ \mathrm{V}) / I(+2\ \mathrm{V}) < -1$ for $LaCl_3$, for the three electrolytes at different concentrations. The absolute values of the rectifications follow the order KCl > $MgCl_2$> $LaCl_3$. Note the shift to low electrolyte concentrations observed in the position of the maxima when the cation charge number increases from z = 1 to 3. We give a qualitative description of the pore charge reversal in the *Appendix A* by using an approximate continuum model.

Figs. 3a and 3b show the *I–V* curves and the rectification ratio of a mixture of electrolytes at different concentrations. In this case, the KCl concentration is fixed to 50 mM while the $MgCl_2$ concentrations are in the range 0 – 100 mM. At concentrations of $MgCl_2$ lower than that of KCl, the presence of Mg^{2+} hardly affects the *I–V* curves. When the $MgCl_2$ concentration approaches 50 mM, however, the positive currents and the rectification ratio decrease with respect to the values obtained at low Mg^{2+} ion concentrations. This fact suggests that at sufficiently high concentrations, the divalent cations are screening a significant fraction of the pore negative charge, thus decreasing its effective value. The

counter-intuitive result here is that the positive current of Fig. 3a can decrease rather than increase with the number of mobile electrical carriers. Note that, in addition to the total concentration of the electrolyte mixture, the effective surface charge density modulates also the pore conductivity [32]. This charge density is decreasing with the magnesium concentration because of the electrical screening, as shown by the decrease observed in the rectification ratio of Fig. 3b.

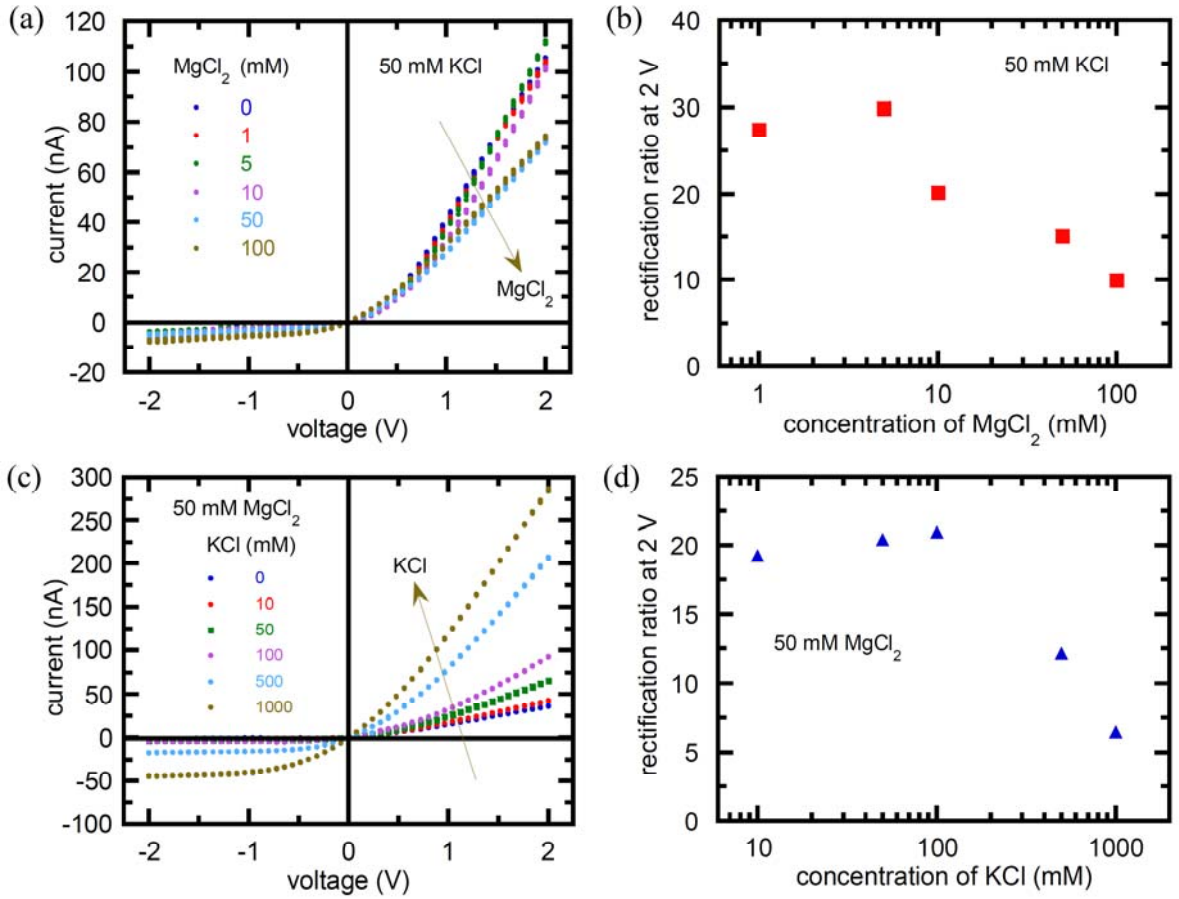

Fig. 3 (a) The *I*–*V* curves of mixtures of electrolytes at different concentrations. The KCl concentration is fixed to 50 mM and the $MgCl_2$ concentrations are changed between 0 and 100 mM. The arrow indicates the direction of increasing $MgCl_2$ concentration. (b) The corresponding rectification ratios. (c) The *I*–*V* curves obtained when the $MgCl_2$ is fixed to 50 mM and the KCl concentrations are increased from 0 to 1000 mM. The arrow indicates the direction of increasing KCl concentration. (d) The corresponding rectification ratios.

Figs. 3c and 3d show the *I*–*V* curves and the rectification ratio of a mixture of electrolytes: $MgCl_2$ is kept constant to 50 mM, while the KCl concentration is changed from 0 to 1000 mM. For comparison, the case of pure KCl at 50 mM is also shown (Fig. 3c). The pore conductance of the pure KCl solution at +2 V is three times higher than that of a pure $MgCl_2$ solution of the same concentration. The divalent ion screening of the negative on the pore surface is significant: Fig. 3c shows that the pore conductance of the pure 50 mM KCl solution is significantly higher than that of an electrolyte mixture with 50 mM $MgCl_2$ + 100 mM KCl despite the increase in the mobile ions. Figs. 3c and 3d also demonstrate that both the positive current and the rectification increase with the KCl concentration up to 100 mM, contrary to the effect shown by Figs. 3a and 3b when the $MgCl_2$ concentration is increased. At KCl concentrations higher than 100 mM, however, the significant screening of the negative pore charges gives a decrease of the rectification ratio (see Fig. 3d).

Figs. 4a and 4b consider the *I*–*V* curves and rectification ratio for the case of an electrolyte mixture composed of 50 mM KCl and $LaCl_3$ concentrations in the range 0 – 50 mM. The presence of small amounts of lanthanum in the solution dramatically modifies the electrical response of the pore compared with the case of magnesium (Fig. 3a). The charge inversion of Fig. 4b suggests that the trivalent ion not only screens the negative charge of the pore, as shown in Fig. 3b for the divalent ion, but can also reverse this charge to positive values at concentrations around 5 mM, in agreement with Fig. 2a. Fig. 4c shows the *I*–*V* curves for a mixture composed of 50 mM $LaCl_3$ and KCl concentrations in the range 0 – 1000 mM. The addition of KCl increases the number of mobile carriers and then the pore conductance. Figs. 4d shows that at KCl concentrations higher than 100 mM, the significant screening of the (now positive) pore charges gives a decrease of the rectification ratio; compare Fig. 4d with Fig. 3d.

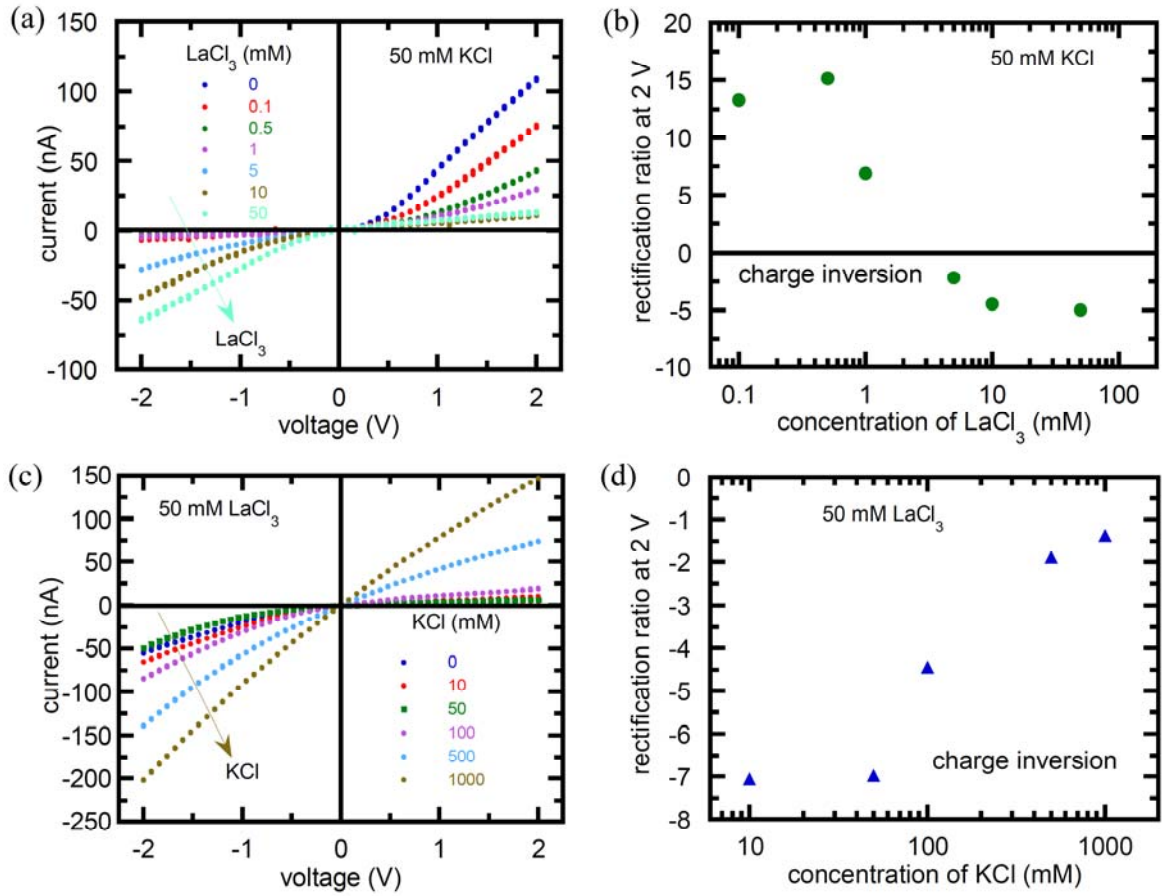

Fig. 4 (a) The *I*–*V* curves of mixtures of electrolytes at different concentrations. The KCl concentration is fixed to 50 mM and the $LaCl_3$ concentrations are changed between 0 and 50 mM. The arrow indicates the direction of increasing $LaCl_3$ concentration. (b) The corresponding rectification ratios. (c) The *I*–*V* curves obtained when the $LaCl_3$ concentration is fixed to 50 mM and the KCl concentrations are increased from 0 to 1000 mM. The arrow indicates the direction of increasing KCl concentration. (d) The corresponding rectification ratios.

The charge inversion of a negatively charged single-colloid has been studied from electrophoretic mobility experiments and molecular dynamics simulations [20]. A mobility reversal is also observed in the presence of La^{3+} ions at ionic strengths larger than 10 mM [20]. The addition of a monovalent salt gives a shift of the colloid isoelectric point to higher lanthanum concentrations (see Fig. 8 of Ref. [20]). A similar effect is also observed for other

trivalent ions in the case of the streaming conductance and the effective surface charge of rectangular silica nanochannels (see Fig. 4 of Ref. [26]). These effects are in qualitative agreement with the screening of the coulombic interactions observed here for the nanopore fixed charges.

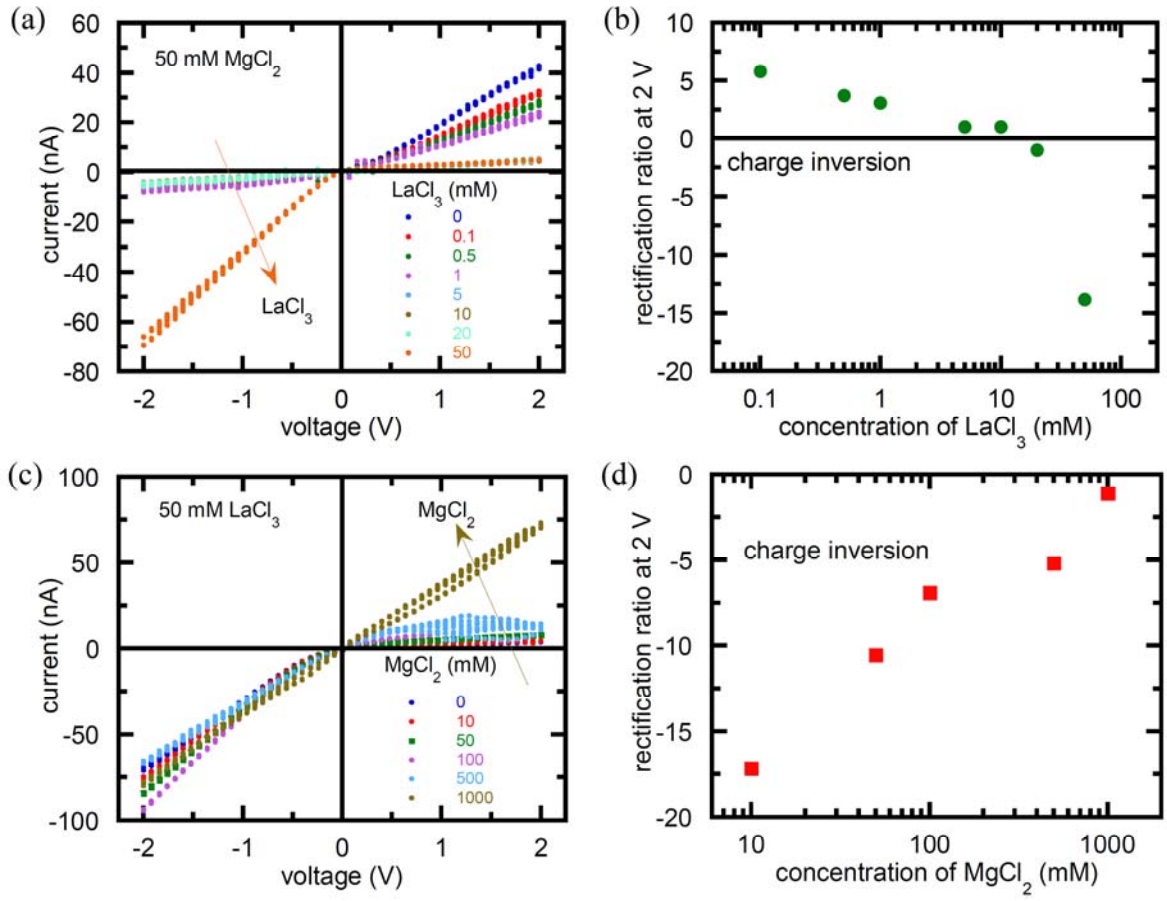

Fig. 5 (a) The *I*–*V* curves of mixtures of electrolytes at different concentrations. The $MgCl_2$ concentration is fixed to 50 mM and the $LaCl_3$ concentrations are changed between 0 and 50 mM. The arrow indicates the direction increasing $LaCl_3$ concentration. (b) The corresponding rectification ratios. (c) The *I*–*V* curves obtained when the $LaCl_3$ concentration is fixed to 50 mM and the $MgCl_2$ concentrations are increased from 0 to 1000 mM. The arrow indicates the direction of increasing $MgCl_2$ concentration. (d) The corresponding rectification ratios.

Figs. 5a and 5b consider the *I*–*V* curves and rectification ratio for the case of a mixture of 50 mM $MgCl_2$ and $LaCl_3$ concentrations in the range 0–50 mM. The addition of La^{3+} cation

reverses also the sign of the pore charge but higher concentrations of this trivalent ion are now needed compared with those of Fig. 4b. Figs. 5c and 5d show the *I*–*V* curves and rectification ratio for a mixture of 50 mM $LaCl_3$ and $MgCl_2$ concentrations in the range 0–1000 mM. Initially, the addition of $MgCl_2$ at increasing concentrations also increases the pore conductance at negative voltages. However, when the $MgCl_2$ concentration is much higher than that of $LaCl_3$ (50 mM), the pore conductance can decrease because of the partial substitution of La^{3+} by Mg^{2+} (see Fig. 2a). Note also the almost complete screening of the positive pore charges and the concomitant decrease of the rectification ratio observed at sufficiently high monovalent salt (KCl) concentrations (see Fig. 4d).

To analyze the ion substitution kinetics in the pore solution, Fig. 6 shows the time recovery of the *I*–*V* curve for a nanopore that was initially immersed in 50 mM $LaCl_3$. At $t = 0$ h, the single-pore membrane is placed in the measuring cell, separating two 100 mM KCl solutions, under the constant action of a input 14 mHz triangular wave of amplitude 2 V. The current passing through the sample is measured at time intervals of hours (h) indicated in Fig. 6. By comparing the resulting curves with those of Fig. 2a for the 100 mM KCl solution, it is concluded that the pore is recovered after 4 h approximately.

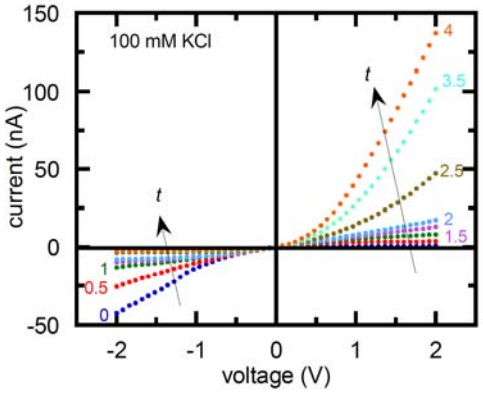

Fig. 6 The recovery of the *I*–*V* curve for a nanopore initially immersed in 50 mM $LaCl_3$. At $t = 0$ h, the single-pore membrane is placed in the measuring cell, separating two 100 mM KCl solutions, under the constant action of an input 14 mHz triangular wave of amplitude 2 V. The

current passing through the sample is then measured at the times (h) indicated close each curve.

Figs. 7a-h show the hysteresis effects observed in the *I–V* curves of different multivalent ions at sufficiently high voltages. In the case of the La^{3+} cation, non-hysteretic (Fig. 7a) and hysteretic (Fig. 7b) behavior can be observed in the range of voltages studied. The pore electrical response depends strongly on the particular sequence of steps followed when the concentration of $LaCl_3$ in the external solutions is changed. The hysteretic behavior is observed usually when the first $LaCl_3$ concentration employed in a series of measurements is relatively low (e.g., 5mM – 10 mM). On the contrary, when the pore is initially equilibrated in more concentrated solutions above 50 mM $LaCl_3$, the *I–V* curves are approximately reproducible down to $LaCl_3$ concentrations as low as 5 mM. Thus, the non-hysteretic behavior appears to require the presence of La^{3+} ions at high enough concentration in the pore solution.

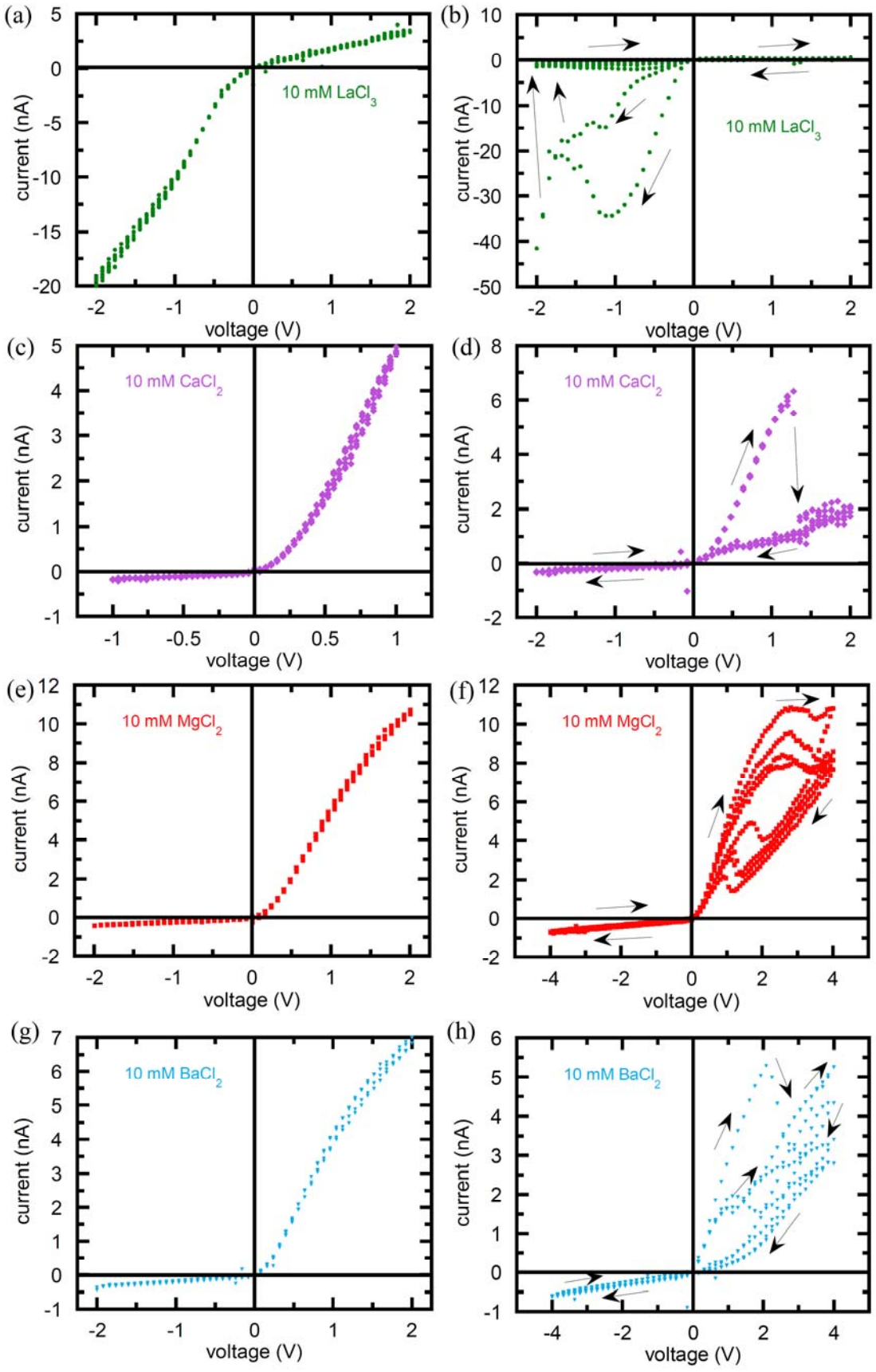

Fig. 7 (a) The *I*–*V* curve of $LaCl_3$ at 10 mM and voltages in the range [–2 V,+2 V]. (b) The

I–*V* curve of $LaCl_3$ can also show a hysteretic behavior for these voltages if the pore has not been equilibrated previously in a $LaCl_3$ solution of concentration above 50 mM. (c) The *I*–*V* curve of $CaCl_2$ at 10 mM and voltages in the range [–1 V,+1 V]. (d) The *I*–*V* curve of $CaCl_2$ at high voltages in the range [–2 V,+2 V] shows a hysteretic behavior. (e) The *I*–*V* curves of $MgCl_2$ at 10 mM and voltages in the range [–2 V,+2 V] (f) The *I*–*V* curves of $MgCl_2$ at high voltages in the range [–4 V,+4 V] shows a hysteretic behavior. (g) The *I*–*V* curves of $BaCl_2$ at 10 mM and voltages in the range [–2 V,+2 V]. (h) The *I*–*V* curves of $BaCl_2$ at high voltages in the range [–4 V,+4 V] shows a hysteretic behavior. The arrows indicate the direction of the measurements with increasing time.

For the case of the divalent ions (Figs. 7c–h), however, we have observed that the hysteresis phenomena do not depend markedly on the sequence of concentrations used, but on the voltage range applied instead. For instance, the *I*–*V* curve of $CaCl_2$ shows no hysteresis at low voltages in the range [–1 V,+1 V] (Fig. 7c) but hysteretic behavior at high voltages in the range [–2 V,+2 V] (Fig. 7d). The *I*–*V* curves of $MgCl_2$ (Figs. 7e and f) and $BaCl_2$ (Figs. 7g and h) can also show hysteresis at voltages higher than those of $CaCl_2$.

It has been shown that relatively small amounts of divalent cations added to a buffered monovalent ionic solution may produce oscillating currents and hysteretic phenomena because of the partial blocking of the conical pore tip [9]. This blocking has been ascribed to the transient formation and re-dissolution of nanoprecipitates [11,37]. However, the experimental conditions used in these studies were not the same as those considered here and then their results cannot be directly extrapolated to our case [37]. While phenomenological schemes to describe qualitatively the voltage-induced current fluctuations through a single nanopore have been proposed in terms of nonlinear dynamics approaches [38] and

electrodiffusion equations [39] the fact is that we have not a definitive theoretical explanation concerning the hysteretic phenomena observed here. Note in this context that our main objective is the effect of charge inversion on the non-hysteretic curves corresponding to mixtures of asymmetric electrolytes.

Figure 8a–f shows the cases of pure $CaCl_2$ (50 mM) for voltages in the ranges [−1 V,+1 V] (Fig. 8a) and [−2 V,+2 V] (Fig. 8b) together with divalent symmetric mixtures of $CaCl_2$ + $MgCl_2$ (25 mM + 25 mM; Fig. 8c and d) and $CaCl_2$ + $BaCl_2$ (25 mM + 25 mM; Fig. 8e and f). The *I*–*V* curves of the mixtures $CaCl_2$ (25 mM) + $MgCl_2$ (25 mM) and $CaCl_2$ (25 mM) + $BaCl_2$ (25 mM) for voltages in the range [−1 V,+1 V] do not show a significant decrease in the pore conductance when compared to Fig. 8a. For voltages in the range [−2 V,+2 V], however, the *I*–*V* curves of the mixtures show also hysteretic behaviors (Fig. 8d and f) due to the presence of Ca^{2+} ions (see Fig. 7d, e, and g together with Fig. 8b). In conclusion, the hysteresis observed in Figs. 7 and 8 points out the qualitative reproducibility of the *I*–*V* curves measured, contrary to the case of the results of Figs. 2–5 that show a quantitative reproducibility.

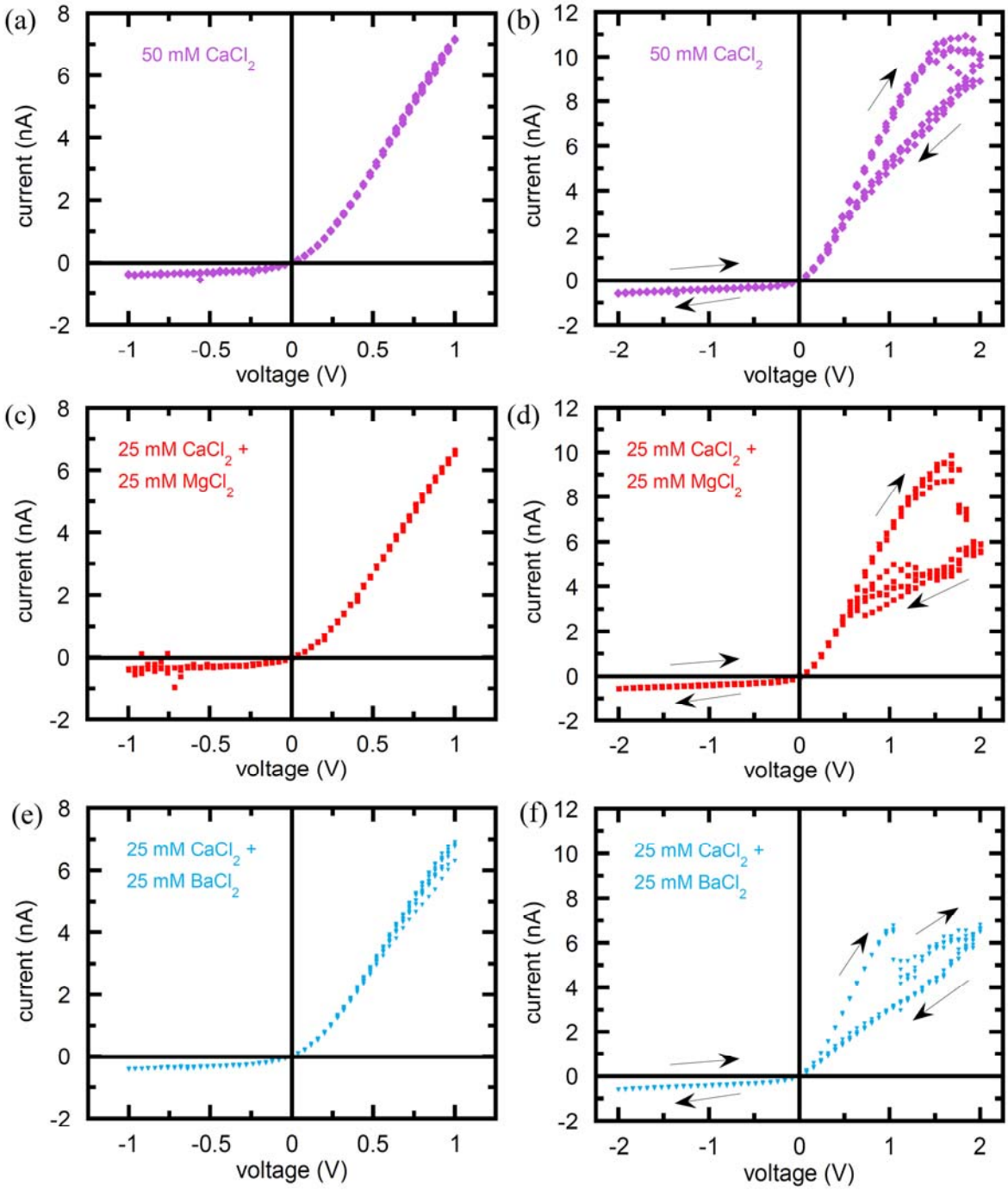

Fig. 8 (a) The *I*–*V* curve of $CaCl_2$ at 50 mM and voltages in the range [–1 V,+1 V]. (b) The *I*–*V* curve of $CaCl_2$ at 50 mM and voltages in the range [–2 V,+2 V] shows a hysteretic behavior. (c) The *I*–*V* curve of the mixture 25 mM $CaCl_2$ + 25 mM $MgCl_2$ and voltages in the range [–1 V,+1 V] does not show a noticeable decrease in the pore conductance when compared to (a). (d) The *I*–*V* curve of the mixture 25 mM $CaCl_2$ + 25 mM $MgCl_2$ and voltages in the range [–2 V,+2 V] shows a hysteretic behavior. (d) The *I*–*V* curve of the

mixture 25 mM $CaCl_2$ + 25 mM $BaCl_2$ and voltages in the range [–1 V,+1 V] does not show a noticeable decrease in the pore conductance when compared to (a). (e) The *I*–*V* curve of the mixture 25 mM $CaCl_2$ + 25 mM $BaCl_2$ and voltages in the range [–2 V,+2 V] shows a hysteretic behavior. The arrows indicate the direction of the measurements with increasing time.

Although we have focused our study on the experimental characterization of the nanopore rectification phenomena, we have also developed a qualitative explanation of the effect of the pore charge overcompensation by lanthanum ion on the current-voltage curves by proposing an ad hoc charge distribution which allows us to estimate the effective charge density (Fig. 9a; see also *Appendix A*). The model gives two reasonable values, $\sigma_{\text{eff}} = +0.086\, e/\text{nm}^2$ at 100 mM $LaCl_3$ and $\sigma_{\text{eff}} = +0.109\, e/\text{nm}^2$ at 50 mM $LaCl_3$, for the effective surface charge densities. The theoretical *I*–*V* curves predicted from this model and the Nernst-Planck ion flux equations (Fig. 9b) show also a qualitative agreement with the experimental results (Fig. 2c).

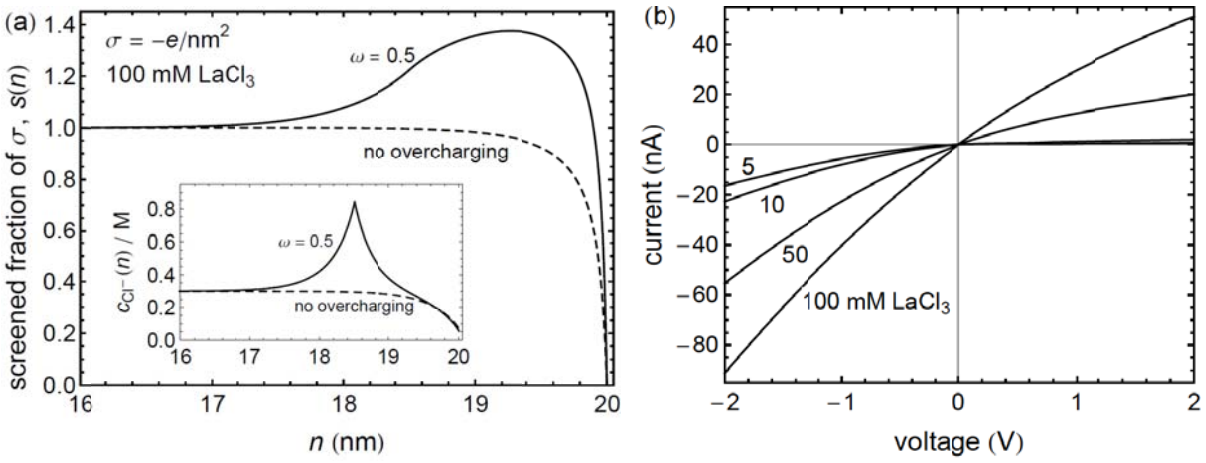

Fig. 9 (a) The fraction $s(n)$ of the actual surface charge $\sigma = -e/\text{nm}^2$ that has been screened at position $n = r\theta$ (normal to the pore surface and measured from its axis) can be larger than 100 % due to the charge overcompensation by trivalent cations. A pore radius $a = 20\,\text{nm}$ has

been considered here. The screening is close to 100 % at a distance of a few Debye lengths, $1/\kappa_D$, from the pore surface. The insets show the coion (chloride) concentration profile. The maximum shown at a distance d = 1.5 nm from the pore surface is in qualitative agreement with the results obtained previously by Monte Carlo simulations [10]. (b) The theoretical *I–V* curves calculated for a conical pore of geometrical characteristics $L = 12.5\,\mu\text{m}$, $a_R = 20\,\text{nm}$, $a_L = 900\,\text{nm}$, and $a_{\text{eff}}(x) = -\delta + a_L + (a_R - a_L)x/L$, with an effective surface charge density $\sigma_{\text{eff}} = +0.1\,e/\text{nm}^2$, are in qualitative agreement with the experimental curves for $LaCl_3$ of Fig. 2c.

3. Conclusions

By studying the *I–V* curves and current rectification ratios, we have described the screening of the negative charges (carboxylic acid groups) fixed on the surface of a conical nanopore by multivalent cations. In particular, we have provided new experimental data and physical insights on the overcompensation of spatially-fixed charges by multivalent ions in confined nanoscale geometries. The *charge inversion* was studied in mixtures of asymmetric electrolytes ($LaCl_3$ and $MgCl_2$ with KCl). Remarkably, small concentrations of multivalent ions allow tuning the nanopore electrical characteristics and the transport of other majority ions present in solution. In particular, pore charge inversion was demonstrated for pure $LaCl_3$ solutions as well as for mixtures of La^{3+} ion at low concentrations with monovalent (K^+) and divalent (Mg^{2+}) ions at biologically relevant concentrations. We have described the kinetics of the nanopore electrical recovery when the electrolyte solutions bathing the single-pore membrane are changed and show the hysteretic effects observed in the *I–V* curves of different multivalent ions in solutions of $CaCl_2$, $MgCl_2$, and $BaCl_2$ and mixtures. Finally, we have given

a qualitative description of the effects of the charge reversal on the pore rectification based on an extended Poisson-Boltzmann formalism and the Nernst-Planck ion flux equations.

Acknowledgments

P. R., J. A. M., J. C., V. G., and S. M. acknowledge the support from European Regional Development Funds and the Ministerio de Economia y Competitividad (project MAT2015-65011-P). M. A., I. P., and W. E. acknowledge the funding from the Hessen State Ministry of Higher Education, Research and the Arts, Germany, under the LOEWE project iNAPO.

TOC image

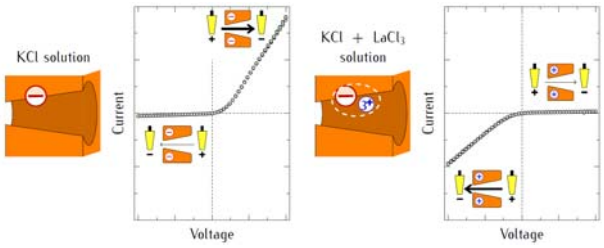
KCl solution
Current
Voltage
KCl + LaCl3
solution
Current
Voltage

Appendix A: Qualitative model for the effect of charge inversion

Trivalent ions tend to accumulate close to pore surface so that they produce a sign reversal of the effective charge density. In general, models based on the Poisson-Boltzmann equation (PBE) cannot explain the overcompensation by multivalent cations [1]. Monte Carlo simulations [10] show that, under overcompensation conditions, the coion concentration shows a local maximum in the neighborhood of the charged surface. Similar ionic concentration profiles can be obtained by the *ad hoc* charge distribution explained below, which determines some boundary conditions on the PBE. This approach it is not intended to explain overcompensation, but only to provide qualitative insights on the effect of the charge inversion on the nanopore rectification.

We consider a nanopore immersed in symmetrical mixed electrolyte solutions of concentrations c_{14}^{b} KCl, c_{24}^{b} $MgCl_2$ and c_{34}^{b} $LaCl_3$; the subscripts for the ionic species are i = 1 K^+, 2 Mg^{2+}, 3 La^{3+}, and 4 Cl^-. Spherical coordinates are used inside the conical nanopore [32]. The Poisson equation in spherical coordinates under azimuthal symmetry is

$$\frac{1}{r^2}\frac{\partial}{\partial r}\left(r^2\frac{\partial \varphi}{\partial r^2}\right)+\frac{1}{r^2\sin\theta}\frac{\partial}{\partial \theta}\left(\sin\theta\frac{\partial \varphi}{\partial \theta}\right)=\rho_{\mathrm{e}} \qquad \text{(A1)}$$

where ρ_{e} is the electrical charge density, $\varphi=-F\phi/RT$, and F, R, and T are the Faraday constant, the gas constant, and the temperature. The first term in the left hand side is much smaller than the second and it is usually neglected in space charge models. In conical nanopores with a small pore opening angle, we use of the small polar angle approximation. Thus, Eq. (A1) reduces to $(\mathrm{d}^2\varphi/\mathrm{d}n^2)+(1/n)(\mathrm{d}\varphi/\mathrm{d}n)=\rho_{\mathrm{e}}$ where $n=r\theta$ is the position coordinate normal to the pore surface. The spherical coordinate r describes the axial position in these nanopores.

The electrical charge density $\rho_{\mathrm{e}}(n)=Fc_4^{\mathrm{b}}(x_1\mathrm{e}^{\varphi}+x_2\mathrm{e}^{2\varphi}+x_3\mathrm{e}^{3\varphi}-\mathrm{e}^{-\varphi})$ compensates the surface charge density $\sigma<0$ of the carboxylic acid groups at the pore surface $n=a(r)$, and

hence global electroneutrality is fulfilled, $\int_0^{a(r)} \rho_e(n) 2\pi n \mathrm{d}n = -2\pi a(r)\sigma$. The potential distribution in the normal direction can be obtained from the PBE

$$\frac{1}{\xi}\frac{\mathrm{d}}{\mathrm{d}\xi}\left(\xi\frac{\mathrm{d}\varphi}{\mathrm{d}\xi}\right) = x_1 \mathrm{e}^{\varphi} + x_2 \mathrm{e}^{2\varphi} + x_3 \mathrm{e}^{3\varphi} - \mathrm{e}^{-\varphi} \tag{A2}$$

where $\xi = \kappa_D n$, $\kappa_D^2 = F^2 c_4^b / \varepsilon_0 \varepsilon_r RT$, ε_0 and ε_r the vacuum permittivity and the dielectric constant, respectively, $x_1 = c_{14}^b / c_4^b$, $x_2 = 2c_{24}^b / c_4^b$, $x_3 = 1 - x_1 - x_2$, and $c_4^b = c_{14}^b + 2c_{24}^b + 3c_{34}^b$. In this *ad hoc* charge distribution model, the PBE is subject to the symmetry condition $\mathrm{d}\varphi / \mathrm{d}\xi\big|_{\xi=0} = 0$ and to

$$\left.\frac{\mathrm{d}\varphi}{\mathrm{d}\xi}\right|_{\kappa_D[a(r)-d]+} - \left.\frac{\mathrm{d}\varphi}{\mathrm{d}\xi}\right|_{\kappa_D[a(r)-d]-} = \omega E_0 \ , \quad \left.\frac{\mathrm{d}\varphi}{\mathrm{d}\xi}\right|_{\kappa_D a(r)} = E_0\left[1 + \omega\left(1 - \frac{d}{a(r)}\right)\right], \tag{A3}$$

where $E_0 = -\kappa_D \sigma / F c_4^b$. The discontinuity of the electric field at $n = a(r) - d$ is associated with a penetrable surface charge density $-\omega\sigma$ that describes the accumulation of trivalent ions at a distance *d* from the surface. This distance depends on the finite size of the hydrated trivalent cations and other steric effects concerning the carboxylic acid chains (we assume *d* = 1.5 nm here). The dimensionless parameter ω could be estimated from the comparison of the experimental *I*–*V* curves and the model predictions. Note that the electric potential, the charge density, and the ionic concentration are continuous variables.

The fraction of the surface charge that has been screened at normal position $n = r\theta$ is

$$s(n) = \frac{\int_n^{a(r)} \rho_e(n') 2\pi n' \mathrm{d}n'}{-2\pi a(r)\sigma} = \frac{1}{\kappa_D a(r) E_0} \int_{\kappa_D n}^{\kappa_D a(r)} (x_1 \mathrm{e}^{\varphi(\xi)} + x_2 \mathrm{e}^{2\varphi(\xi)} + x_3 \mathrm{e}^{3\varphi(\xi)} - \mathrm{e}^{-\varphi(\xi)}) \xi \mathrm{d}\xi \ . \tag{A4}$$

The effective charge density at position $a_{\mathrm{eff}} \le a$ is $\sigma_{\mathrm{eff}} = [1 - s(a_{\mathrm{eff}})]\sigma a / a_{\mathrm{eff}}$, so that $\int_0^{a_{\mathrm{eff}}} \rho_e(n) 2\pi n \mathrm{d}n = -2\pi a_{\mathrm{eff}} \sigma_{\mathrm{eff}}$. For example, the value $\omega = 0.5$ would give the sign-reversed, effective charge densities $\sigma_{\mathrm{eff}} = +0.086 e / \mathrm{nm}^2$ for 100 mM $LaCl_3$ and $\sigma_{\mathrm{eff}} = +0.109 e / \mathrm{nm}^2$ for 50 mM $LaCl_3$, calculated at $a_{\mathrm{eff}} = (20 - 2)\ \mathrm{nm} = 18\ \mathrm{nm}$. The above formalism allows

obtaining the curves of Fig. 9a. The *I*–*V* curves of Fig. 9b are calculated by solving the Nernst-Planck equations (*Appendix B*).

Appendix B: Transport equations for multivalent mixed electrolytes

Recently, the conductance curves of single carbon nanotubes have been experimentally [40] and theoretically [41] analyzed, with emphasis on the proton binding chemical affinity. We consider here the case of a conical nanopore immersed in symmetrical solutions of mixed electrolytes with a common univalent anion (–). The concentrations of the $z_1:1$ and $z_2:1$ electrolytes are c_1^{b} and c_2^{b}, respectively. The Nernst-Planck equations for ion transport along the pore are [32]

$$-\frac{\langle J_i\rangle}{D_i}=\frac{\mathrm{d}\langle c_i\rangle}{\mathrm{d}r}+z_i c_i\frac{\mathrm{d}\langle\phi\rangle}{\mathrm{d}r},\quad i=1,2,- \tag{B1}$$

where $\langle\phi\rangle$ is the potential scaled by RT/F. The electroneutrality condition in a section is

$$z_1\langle c_1\rangle+z_2\langle c_2\rangle-\langle c_-\rangle=X(r). \tag{B2}$$

These transport equations are transformed to [42,43]

$$\frac{\mathrm{d}\langle\phi\rangle}{\mathrm{d}r}=-\frac{G_1+\mathrm{d}X/\mathrm{d}r}{S_2},\quad \frac{\mathrm{d}c_{\mathrm{T}}}{\mathrm{d}r}=-G_0+X\frac{G_1+\mathrm{d}X/\mathrm{d}r}{S_2},\quad \frac{\mathrm{d}S_2}{\mathrm{d}r}=-G_2+S_3\frac{G_1+\mathrm{d}X/\mathrm{d}r}{S_2} \tag{B3}$$

where

$$c_{\mathrm{T}}\equiv\langle c_1\rangle+\langle c_2\rangle+\langle c_-\rangle,\quad S_2\equiv z_1^2\langle c_1\rangle+z_2^2\langle c_2\rangle+\langle c_-\rangle \tag{B4}$$

$$G_0\equiv\frac{\langle J_1\rangle}{D_1}+\frac{\langle J_2\rangle}{D_2}+\frac{\langle J_-\rangle}{D_-},\ G_1\equiv\frac{z_1\langle J_1\rangle}{D_1}+\frac{z_2\langle J_2\rangle}{D_2}-\frac{\langle J_-\rangle}{D_-},\ G_2\equiv\frac{z_1^2\langle J_1\rangle}{D_1}+\frac{z_2^2\langle J_2\rangle}{D_2}+\frac{\langle J_-\rangle}{D_-} \tag{B5}$$

$$S_3(c_{\mathrm{T}},S_2)\equiv z_1^3\langle c_1\rangle+z_2^3\langle c_2\rangle-\langle c_-\rangle=(z_1+z_2-1)S_2+(z_1+z_2-z_1z_2)X-z_1z_2c_{\mathrm{T}}. \tag{B6}$$

The boundary conditions are

$$c_{\mathrm{T}}(r_i) = c_1^{\mathrm{b}} \mathrm{e}^{-z_1 \Delta\phi_{\mathrm{D},i}} + c_2^{\mathrm{b}} \mathrm{e}^{-z_2 \Delta\phi_{\mathrm{D},i}} + (z_1 c_1^{\mathrm{b}} + z_2 c_2^{\mathrm{b}}) \mathrm{e}^{\Delta\phi_{\mathrm{D},i}},$$

$$S_2(r_i) = z_1^2 c_1^{\mathrm{b}} \mathrm{e}^{-z_1 \Delta\phi_{\mathrm{D},i}} + z_2^2 c_2^{\mathrm{b}} \mathrm{e}^{-z_2 \Delta\phi_{\mathrm{D},i}} + (z_1 c_1^{\mathrm{b}} + z_2 c_2^{\mathrm{b}}) \mathrm{e}^{\Delta\phi_{\mathrm{D},i}} \quad , \; i = \mathrm{L}, \mathrm{R} \tag{B7}$$

where the Donnan interfacial potential drops $\Delta\phi_{\mathrm{D},i} \equiv \langle\phi\rangle(r_i) - \phi_i$ are found as the solutions of the electroneutrality conditions at the pore boundaries, i = L, R,

$$X(r_i) = z_1 c_1^{\mathrm{b}} \mathrm{e}^{-z_1 \Delta\phi_{\mathrm{D},i}} + z_2 c_2^{\mathrm{b}} \mathrm{e}^{-z_2 \Delta\phi_{\mathrm{D},i}} - (z_1 c_1^{\mathrm{b}} + z_2 c_2^{\mathrm{b}}) \mathrm{e}^{\Delta\phi_{\mathrm{D},i}}. \tag{B8}$$

When the nanopore is immersed in a z:1 electrolyte, a similar transformation leads to

$$\frac{\mathrm{d}c_{\mathrm{T}}}{\mathrm{d}r} = -G_0 + X \frac{\Gamma G_0 + \mathrm{d}X/\mathrm{d}r}{(z-1)X + z c_T} \tag{B9}$$

$$\frac{\mathrm{d}\langle\phi\rangle}{\mathrm{d}r} = -\frac{\Gamma G_0 + \mathrm{d}X/\mathrm{d}r}{(z-1)X + z c_T} \tag{B10}$$

where $c_{\mathrm{T}} \equiv \langle c_+ \rangle + \langle c_- \rangle$, $G_0 \equiv \langle J_+ \rangle / D_+ + \langle J_- \rangle / D_-$, $G_1 \equiv z\langle J_+ \rangle / D_+ - \langle J_- \rangle / D_-$ and $\Gamma \equiv G_1 / G_0$. The boundary conditions are $c_{\mathrm{T}}(r_i) = c^{\mathrm{b}}(\mathrm{e}^{-z\Delta\phi_{\mathrm{D},i}} + z\mathrm{e}^{\Delta\phi_{\mathrm{D},i}})$, where $\Delta\phi_{\mathrm{D},i} \equiv \langle\phi\rangle(r_i) - \phi_i$ are found as the solutions of $X(r_i) = zc^{\mathrm{b}}(\mathrm{e}^{-z\Delta\phi_{\mathrm{D},i}} - \mathrm{e}^{\Delta\phi_{\mathrm{D},i}})$ at the pore boundaries, i = L, R.

The solution procedure is as follows. For a given G_0, we guess Γ, integrate Eq. (B9) from r_{L} using the boundary value $c_{\mathrm{T}}(r_{\mathrm{L}})$, and iterate Γ until the boundary condition at r_{R} is fulfilled. The current density is then $I = F\left(z\langle J_+ \rangle - \langle J_- \rangle\right)$, where $\langle J_+ \rangle = D_+ G_0 (1+\Gamma)/(1+z)$ and $\langle J_- \rangle = D_- G_0 (z-\Gamma)/(1+z)$. Finally, the potential drop in the nanopore is $\Delta\langle\phi\rangle = \int_{r_{\mathrm{L}}}^{r_{\mathrm{R}}} (\mathrm{d}\langle\phi\rangle/\mathrm{d}r)\mathrm{d}r$ and the applied potential is $V \equiv \phi_{\mathrm{L}} - \phi_{\mathrm{R}} = \Delta\phi_{\mathrm{D,R}} - \Delta\phi_{\mathrm{D,L}} - \Delta\langle\phi\rangle$.

References

[1] A. Y. Grosberg, T. T. Nguyen, B. I. Shklovskii, Colloquium: The physics of charge inversion in chemical and biological systems, Rev. Mod. Phys. 74 (2002) 329–345.

[2] B. Hille, Ion Channels of Excitable Membranes, Sinauer Associates, Sunderland, 1992.

[3] D. Fologea, E. Krueger, R. Al Faori, R. Lee, Y. I. Mazur, R. Henry, M. Arnold, G. J. Salamo, Multivalent ions control the transport through lysenin channels. Biophys. Chem. 152 (2010) 40–45.

[4] P. A. Gurnev, S. M. Bezrukov, Inversion of membrane surface charge by trivalent cations probed with a cation-selective channel, Langmuir 28 (2012) 15824−15830.

[5] M. Queralt-Martin, E. García-Gimenez, S. Mafe, A. Alcaraz, Divalent cations reduce the pH sensitivity of OmpF channel inducing the pK_a shift of key acidic residues, Phys. Chem. Chem. Phys. 13 (2011) 563–569.

[6] C. Verdia-Baguena, M. Queralt-Martin, V. M. Aguilella, A. Alcaraz, Protein ion channels as molecular ratchets. Switchable current modulation in outer membrane protein F porin induced by millimolar La^{3+} ions, J. Phys. Chem. C 116 (2012) 6537−6542.

[7] M. Queralt-Martin, C. Verdia-Baguena, V. M. Aguilella, A. Alcaraz, Electrostatic interactions drive the nonsteric directional block of OmpF channel by La^{3+}, Langmuir 29 (2013) 15320−15327.

[8] M. Lidón López, María Queralt-Martín, Antonio Alcaraz, Experimental demonstration of charge inversion in a protein channel in the presence of monovalent cations, Electrochem. Comm. 48 (2014) 32–34.

[9] Z. S. Siwy, M. R. Powell, E. Kalman, R. D. Astumian, R. S. Eisenberg, Negative incremental resistance induced by calcium in asymmetric nanopores, Nano Lett. 6 (2006) 473–477.

[10] Y. He, D. Gillespie, D. Boda, I. Vlassiouk, R. S. Eisenberg, Z. S. Siwy, Tuning transport properties of nanofluidic devices with local charge inversion, J. Am. Chem. Soc. 131 (2009) 5194–5202.

[11] L. Innes, M. R. Powell, I. Vlassiouk, C. Martens, Z. S. Siwy, Precipitation-induced voltage-dependent ion current fluctuations in conical nanopores, J. Phys. Chem. C 114 (2010) 8126–8134.

[12] M. Ali, S. Nasir, P. Ramirez, J. Cervera, S. Mafe, W. Ensinger, Calcium binding and ionic conduction in single conical nanopores with polyacid chains: Model and experiments, ACS Nano 6 (2012) 9247– 9257.

[13] H. Yao, Y. Cheng, J. Zeng, D. Mo, J. Duan, J. Liu, P. Zhai, Y. Sun, J. Liu, Bivalent ion transport through graphene/PET nanopore. Appl. Phys. A 122 (2016) 509.

[14] J. Lyklema, Overcharging, charge reversal: Chemistry or physics?, Colloids Surf. A 291 (2006) 3–12.

[15] Z.-Y. Wang, J. Wu, Ion association at discretely-charged dielectric interfaces: Giant charge inversion, J. Chem. Phys. 147 (2017) 024703.

[16] O. Lenz, C. Holm, Simulation of charge reversal in salty environments: Giant overcharging?, Eur. Phys. J. E 26 (2008) 191–195.

[17] A. G. Albesa, M. Rafti, J. L. Vicente, Trivalent cations switch the selectivity in nanopores, J. Mol. Model. 19 (2013) 2183–2188.

[18] M. Quesada-Perez, A. Martin-Molina, R. Hidalgo-Alvarez, Simulation of electric double layers undergoing charge inversion: Mixtures of mono and multivalent ions, Langmuir 21 (2005) 9231–9237.

[19] Z.-Y. Wang, Y.-Q. Ma, Insights from Monte Carlo simulations on charge inversion of planar electric double layers in mixtures of asymmetric electrolytes, J. Chem. Phys. 133 (2010) 064704.

[20] I. Semenov, S. Raafatnia, M. Sega, V. Lobaskin, C. Holm, F. Kremer, Electrophoretic mobility and charge inversion of a colloidal particle studied by single-colloid electrophoresis and molecular dynamics simulations, Phys. Rev. E 87 (2013) 022302.

[21] M. Quesada-Perez, E. Gonzalez-Tovar, A. Martın-Molina, M. Lozada-Cassou, R. Hidalgo-Alvarez, Overcharging in colloids: beyond the Poisson-Boltzmann approach, ChemPhysChem 4 (2003) 234–248.

[22] J. Pittler,W. Bu, D. Vaknin, A. Travesset, D. J. McGillivray, M. Lösche, Charge inversion at minute electrolyte concentrations, Phys. Rev. Lett. 97 (2006) 046102.

[23] K. Besteman, M. A. G. Zevenbergen, H. A. Heering, S. G. Lemay, Direct observation of charge inversion by multivalent ions as a universal electrostatic phenomenon, Phys. Rev. Lett. **93** (2004) 170802.

[24] G. Perez-Mitta, A. G. Albesa, M. E. Toimil Molares, C. Trautmann, O. Azzaroni, The influence of divalent anions on the rectification properties of nanofluidic diodes: Insights from experiments and theoretical simulations, ChemPhysChem 17 (2016) 2718–2725.

[25] S. X. Li, W. Guan, B. Weiner, M. A. Reed, Direct observation of charge inversion in divalent nanofluidic devices, Nanolett. 15 (2015) 5046−5051.

[26] F. H. J. van der Heyden, D. Stein, K. Besteman, S. G. Lemay, C. Dekker, Charge inversion at high ionic strength studied by streaming currents, Phys. Rev. Lett. 96 (2006) 224502.

[27] S. Abdu, M.-C. Martí-Calatayud, J. E. Wong, M. García-Gabaldón, M.Wessling, Layer-by-layer modification of cation exchange membranes controls ion selectivity and water splitting, ACS Appl. Mater. Interfaces 6 (2014) 1843−1854.

[28] Z. Siwy, D. Dobrev, R. Neumann, C. Trautmann, K. Voss, Electro-responsive asymmetric nanopores in polyimide with stable ion-current signal, Appl. Phys. A 76 (2003) 781–785.

[29] P. Apel, Track etching technique in membrane technology, Radiat. Meas. 34 (2001) 559–566.

[30] M. Ali, B. Schiedt, K. Healy, R. Neumann, W. Ensinger, Modifying the surface charge of single track-etched conical nanopores in polyimide. Nanotechnology 19 (2008), 085713.

[31] P. Ramirez, V. Garcia-Morales, V. Gomez, M. Ali, S. Nasir, W. Ensinger, S. Mafe, Hybrid circuits with nanofluidic diodes and load capacitors, Phys. Rev. Applied 7 (2017) 064035.

[32] J. Cervera, B. Schiedt, R. Neumann, S. Mafe, P. Ramirez, Ionic conduction, rectification, and selectivity in single conical nanopores, J. Chem. Phys. 124 (2006) 104706.

[33] P. Ramirez, P. Yu. Apel, J. Cervera and S. Mafe, Pore structure and function of synthetic nanopores with fixed charges: Tip shape and rectification properties, Nanotechnology 19 (2008) 315707.

[34] D. Wang, W. Brown, Y. Li, M. Kvetny, J. Liu, G. Wang, Correlation of ion transport hysteresis with the nanogeometry and surface factors in single conical nanopores, Anal. Chem. 89 (2017) 11811−11817.

[35] D. Momotenko, H. H. Girault, Scan-rate-dependent ion current rectification and rectification inversion in charged conical nanopores, J. Am. Chem. Soc. 133 (2011) 14496−14499.

[36] J. Wei, G. Du, J. Guo, Y. Li. W. Liu, H. Yao. J. Zhao, R.Wu, H. Chen, A. Ponomarov, The rectification of mono- and bivalent ions in single conical nanopores, Nucl. Instrum. Methods Phys. Res. Sect. B 404 (2017) 219–223

[37] M. R. Powell, M. Sullivan, I. Vlassiouk, D. Constantin, O. Sudre, C. C. Martens, R. S. Eisenberg, Z. S. Siwy, Nanoprecipitation-assisted ion current oscillations, Nature Nanotechnol. 3 (2008) 51–57.

[38] B. Hyland, Z. S. Siwy, C. C. Martens, Nanopore current oscillations: Nonlinear dynamics on the nanoscale, J. Phys. Chem. Lett. 6 (2015) 1800–1806.

[39] M.-T. Wolfram, M. Burger, Z. S. Siwy, Mathematical modeling and simulation of nanopore blocking by precipitation, J. Phys.: Condens. Matter 22 (2010) 454101.

[40] E. Secchi, A. Niguès, L. Jubin, A. Siria, L. Bocquet, Scaling Behavior for Ionic Transport and its Fluctuations in Individual Carbon Nanotubes, Phys. Rev. Lett. 116 (2016) 154501.

[41] P. M. Biesheuvel, M. Z. Bazant, Analysis of ionic conductance of carbon nanotubes, Phys. Rev. E 94 (2016) 050601(R).

[42] J. A. Manzanares, K. Kontturi, Diffusion and migration, in Encyclopedia of Electrochemistry, A. J. Bard, M. Startmann (Eds.), Wiley-VCH, Weinheim, 2003, p. 81.

[43] V. Nikonenko, M. K. Urtenov, Analysis of electrodiffusion equations in the decomposition form, Russ. J. Electrochem. 32 (1996) 187-194.